Properties of Copolymer-Type Polyacetal/Polyurethane Blends

WEN-YEN CHIANG and MING-SONG LO, *Department of Chemical Engineering, Tatung Institute of Technology, 40 Chungshan North Road, 3rd Sec., Taipei 10451, Taiwan, Republic of China*

Synopsis

Mechanical and physical properties of the blends of copolymer-type polyacetals (POM) with polyurethane (PU) were investigated. The properties relationships of POM/PU blends are established by studying their morphology and compatibility. For the blends rich in POM, the morphology of the blends observed with a scanning electron microscopy (SEM) indicates that the blends containing lower than 50 wt % (46 vol %) PU are almost completely filled with spherical particles of the dispersed PU. As the concentration of PU increases, the spherulites of the POM observed by SEM become less perfect with coarse fine structure. Furthermore, when the concentration of PU was increased up to 50 wt %, the spherulites of POM in the blends are smaller than those of unblended POM. X-ray diffraction studies reveal that the degree of crystallinity of POM decreases with increasing PU content, which is nonmonotonic. This conclusion agrees with the observations made by differential scanning calorimetry (DSC) and density measurements. For the blends rich in POM, mechanical properties show that the impact strength of POM/PU blends increased with decreasing spherical size of the dispersed PU.

INTRODUCTION

The concept of physical blending of two or more polymers to obtain new products is now attracting widespread interest.[1-12] Miscible polymer blends recently reached an attractive position in polymer science and technology.[1,5,8] Most commercial multicomponent polymer systems are two-phase blends that display specific advantages over those expected for a single phase system. The morphology of polyblends[1-9,13,14] depends on the arrangement of the phases, whether continuous or discontinuous, and the degree of order in the phases, namely, crystalline or amorphous. In all cases, the importance of the interphase is generally accepted. It should be stressed that the morphology of multiphase polymeric systems has a primary effect on its properties.[1-4] Thus, the improvement in impact strength of brittle polymers is a convincing example. For low-density polyethylene (LDPE) and polypropylene (PP), where LDPE is the disperse phase and PP the matrix, Teh[3] considered LDPE as the soft rubbery phase improving the impact resistance. Also he reported that the spherulitic size of PP decreases when blended with LDPE. The incorporation of ethylene–propylene copolymer and polyisobutylene in PP resulted in an enhanced nucleation rate and a decrease in average size of spherulites as reported by Martuscelli et al.[6]

This paper, using melt blending to make good polyblends, describes an investigation of the properties of copolymer-type polyacetal (POM) and polyether-based polyurethane (PU) blends at three different compositions. Differ-

Journal of Applied Polymer Science, Vol. 36, 1685–1700 (1988)

CCC 0021-8995/88/071685-16$04.00

ential scanning calorimetry (DSC), dynamic viscoelasticity, and scanning electron microscopy (SEM) were used to detect the compatibility and morphology of the blends. Blending with PU is expected to give an alloy material with improved toughness. Understanding the mechanical and physical properties, thermal behavior, and morphology of such alloys is relevant to their processing and product development.

EXPERIMENTAL

Materials

Two commercial copolymer-type polyacetals, Duracon M-90 (POM-I) and Duracon M-270 (POM-II), with melt flow indices of 9.0 and 30.5, and one commercial polyether-based polyurethane (PU), Estane 58300, made by B.F. Goodrich Chemical Co., were used.

Melt Blends

Three different compositions of POM-I/PU and POM-II/PU were compounded at weight ratios of 90/10, 75/25, and 50/50. They were blended in a Brabender Plasti-Corder Model PLE 330 with roller mixer, Type W 50 EC, at 180°C and a speed of 60 rpm for 5 min. The range of equilibrium torques for the melt blends were from 12 to 15 NM. Test specimens were prepared by compression molding in a frame. Each compound was compressed at 150 kg/cm^2 for 5 min and cooled at 75°C/min, from the melt at 180°C to the solid at 23°C.

X-Ray Measurements

The X-ray diffraction profiles were measured on a Rigaku vertical goniometer using FeK_α radiation generated at 50 kV and 40 mA. A teletype was connected to the terminal of the digital counter so that the number of counts was automatically recorded. Intensities were counted at 0.05–1.0° intervals at the Bragg angle of 2θ. The degree of crystallinity (X_c) was calculated from the diffraction peak by determining the ratio of the crystalline area to the total area. The X-ray diffraction from a two-phase model is assumed to be additive. The diffracted intensity is

$$X_c\,(\%) = (I_c/I) \times 100\%$$

where X_c is the degree of crystallinity, I_c is the intensity area between 27° and 30° at the Bragg angle of 2θ, and I is the intensity of the total area from 19° to 35° at the Bragg angle of 2θ. Perfect crystals give narrow diffraction peaks, whereas semicrystalline polymers show broad diffraction peaks. This broadness is interpreted as resulting from the small imperfections of the polymer crystals. The error of X_c in the measurement was between 0.5 and 1.5%.

Mechanical Measurements

Tensile properties were measured with the ASTM D638 test method by an Instron universal testing machine Model 1130. The crosshead load was at 500

kg and a speed of 5 cm/min and chart speed of 100 cm/min. Notched Izod impact strength was measured with the ASTM D256 test method by using Izod type specimens with a thickness of about 0.4 ± 0.02 cm and an energy of 60 kg cm. Mold shrinkage was measured with the ASTM D995 test method. The standard deviations of all mechanical property measurement were ±2.8%.

Density Measurements

The density was calculated from specific gravity measured at 23°C with the ASTM D792. The calculation was based on the following:

$$\text{sp gr } 23/23°\text{C} = a/(a + w - b)$$

where a is the apparent weight of the specimen without a wire or sinker in air, b is the apparent weight of the specimen (and of the sinker) completely immersed and of the wire partially immersed in distilled water, and w is the apparent weight of the totally immersed sinker and of the partially immersed wire. Thus, the density of POM was calculated from

$$D\ (\text{g/cm}^3) = \text{sp gr } 23/23°\text{C} \times 0.9975$$

The error of density measurement was between 0.5 and 2.0%.

Dielectric Dissipation Factor Measurements

The dielectric dissipation factor ($\tan \delta$) of the POM samples, which were molded into sheet specimens of 1.5 mm thickness, were measured by the capacitance and arc loss at a frequency of 1 MHz (ASTM D150):

$$\tan \delta = K''/K'$$

where K'' is the loss index and K' is the relative permittivity. The error of $\tan \delta$ in the measurement was between 0.5 and 4.5%.

Thermal Analysis

A DuPont 910 differential scanning calorimeter was used to study thermal history. About 1.20–2.20 mg of polymer sample was melted at 200°C for at least 5 min and then cooled to 30°C at 5°C/min in nitrogen to allow the polymer to crystallize. The melting point was observed, and the melting enthalpy (H_f) was calculated by integrating the area under the melting endotherm of the DSC trace using the equation

$$H_f = (A \times B \times E \times S)/M$$

where A is the peak area (cm^2) under the curve, B is the time base unit (min/cm), E is the cell calibration coefficient, S is the sensitivity (J/min cm), and M is the sample weight (g).

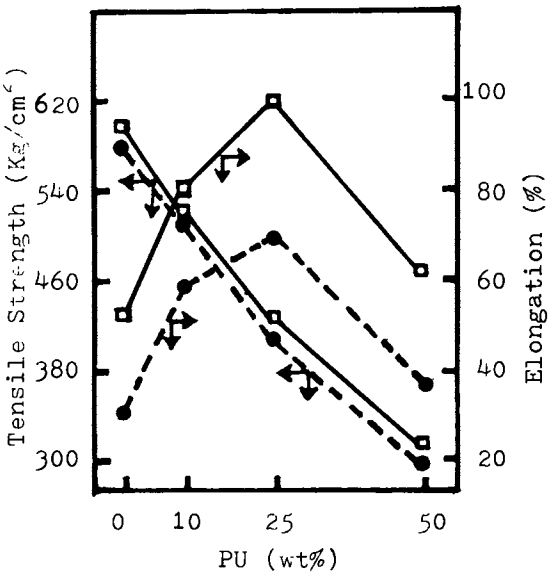

Fig. 1. Tensile strength and elongation at break of POM/PU blends: (———) POM-I/PU blend; (- - - -) POM-II/PU blend.

Dynamic Viscoelasticity

Dynamic viscoelasticity: damping, storage modulus (E'), and loss modulus (E'') were measured in a Rheovibron DDV II dynamic viscoelastometer at a heating rate of 1–2°C/min and a frequency of 11 Hz in the temperature range from −110 to 90°C. The test specimens were made from a rectangular strip about 4–7 cm long with the thickness: 0.006 cm for POM, 0.010 cm for POM/PU = 90/10 wt % blend, 0.015 cm for POM/PU = 75/25 wt % blend, and 0.025 cm for POM/PU = 50/50 wt % blend.

SEM Photographs

Scanning electron micrographs (SEM) of the cryofracture surfaces of samples in the liquid nitrogen were taken on a Cambridge Stereoscan Mark II 150 with a gold coating of 150 Å thickness.

RESULTS AND DISCUSSION

Mechanical Properties

In POM/PU blends rich in POM, a two-phase polymeric system is important for the stress–strain behavior in at least one major area of applications, namely, the rubbery PU phase is added to the brittle POM matrix to increase the toughness and elongation to break of the POM polymer. The tensile strength at break is plotted as function of composition in Figure 1, which decreases with increasing concentration of PU. Also, the elongation of the blends reaches a maximum at 25 wt % PU (Fig. 1). As the composition of PU was increased in the blend, the crystallinity of the blend decreases. Thus, Young's modulus and mold shrinkage of the blend decrease with increasing

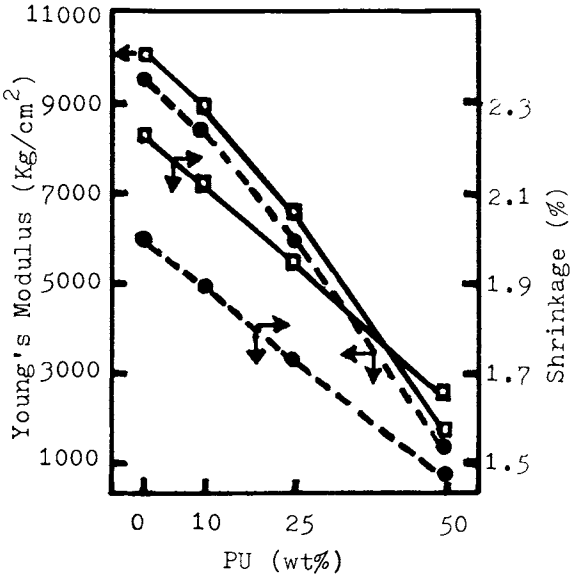

Fig. 2. Young's modulus and mold shrinkage of POM/PU blends: (———) POM-I/PU blend; (- - - -) POM-II/PU blend.

PU content, as shown in Figure 2. Lipatov[15] reported that mechanical characteristics are associated with interpenetration of the additive component into the surface defects of the bulk component.

Impact strength increases with the amount of PU in the POM matrix up to 10 wt % limiting value,[16,17] and then decreases, as shown in Figure 3. The PU rubber particles often are spherical with spherical inclusions[18,19] of the POM

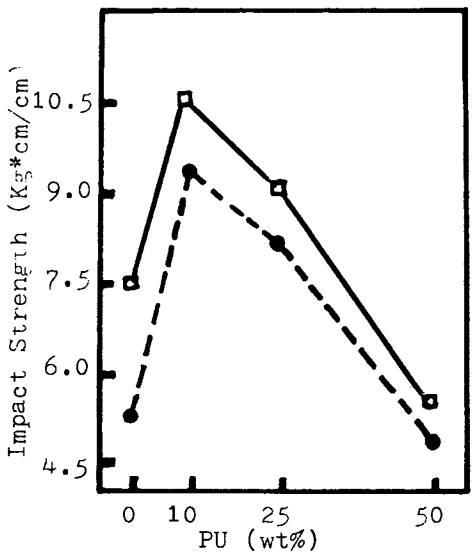

Fig. 3. Notched Izod impact strength of POM/PU blends: (———) POM-I/PU blend; (- - - -) POM-II/PU blend.

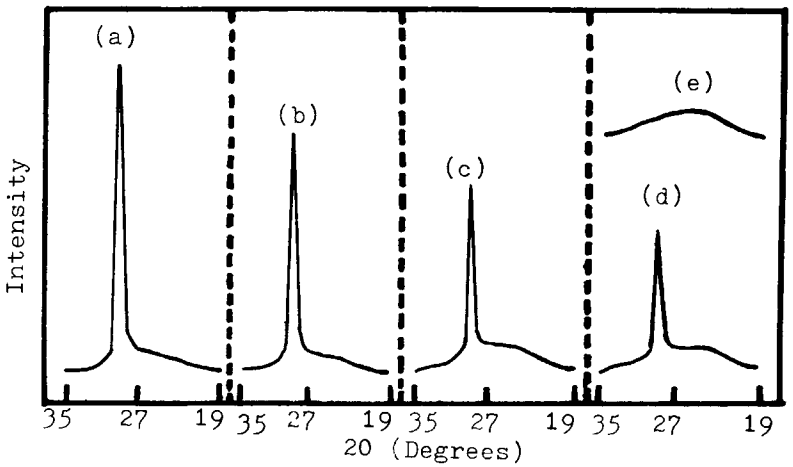

Fig. 4. Radial intensity distribution: (a) pure POM-I; (b) POM-I/PU = 90/10 wt %; (c) POM-I/PU = 75/25 wt %; (d) POM-I/PU = 50/50 wt %; (e) pure PU.

rigid phase. PU as a dispersed phase will be distributed in the continuous phase of POM, and acts as an energy absorber to improve impact strength of the blend. At a concentration larger than 25 wt % of the rubbery phase, the dispersed particles tend to agglomerate or to form elongated rather than spherical particles. At this point an inversion of the phases starts, accompanied by a rapid decrease in Young's modulus (Fig. 2). Thus the POM/PU (50/50 wt %) blend reaches a minimum value of Izod impact strength. Because a compatible blend might have a profound effect on toughness

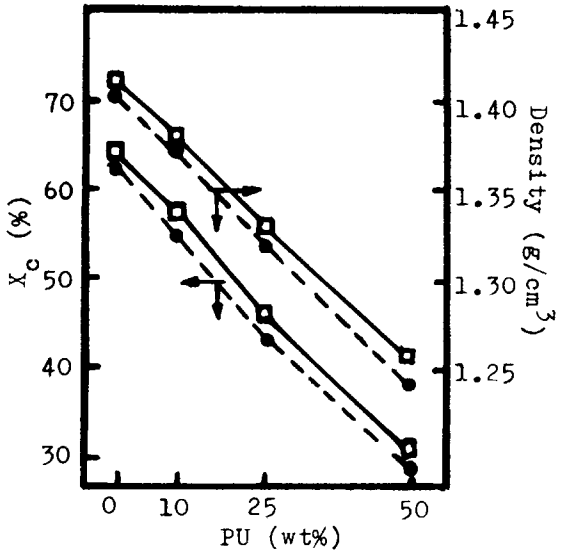

Fig. 5. Degree of crystallinity (X_c) and density of POM/PU blends: (———) POM-I/PU blend; (- - - -) POM-II/PU blend.

improvement without sacrificing the strength remarkably, the extent of impact strength increase correlated well with the PU content.

Physical Properties

The wide-angle X-ray diffraction (WAXD) studies show that the angle position of the specific reflection remains unchanged at POM/PU blends rich in POM. In Figure 4, the diffraction lines measured at half POM maximum intensity are observed to be independent of composition, suggesting that there is no change in the crystal lamellar thickness.[20] The figure shows the plot of the relative intensities of the maximum X-ray diffraction peaks as a function of composition. The degree of crystallinity of the alloys by applying the two-phase model[21] decreases with increasing concentration of PU and the density (Fig. 5). Within the range of small concentration of PU additives, the density and crystallinity of the blend is similar to the additive value for the blend. When the concentration of PU is larger than 10 wt %, it can be related to the surplus free volume, located at the interphase border because of the incompatibility of the components. With further increase in PU content, the density and crystallinity of the blends becomes lower (Fig. 5). Therefore, the density and crystallinity of the blends are nonmonotonic.[19,21]

Dielectric Dissipation Factor (tan δ)

The crystallinity of the blend decreases with increasing concentration of PU acting as stress concentrator. Thus the lower crystallinity should result in a higher dielectric dissipation factor (tan δ) in the blend of POM/PU = 50/50 wt %, as shown in Figure 6, which is due to the presence of greater amount of PU phase in the POM matrix because of denser packing between the lamellae

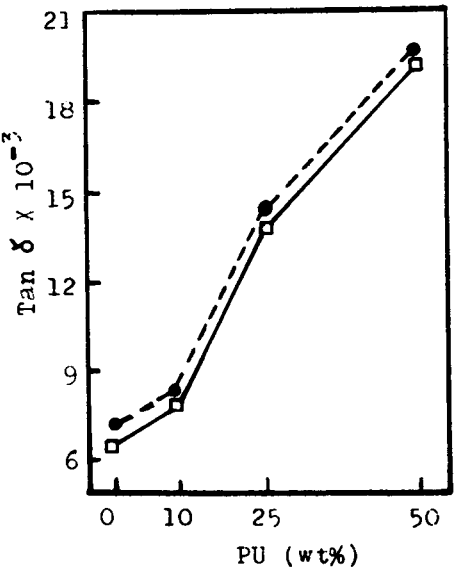

Fig. 6. Dielectric dissipation factor (tan δ) of POM/PU blends: (———) POM-I/PU blend; (- - - -) POM-II/PU blend.

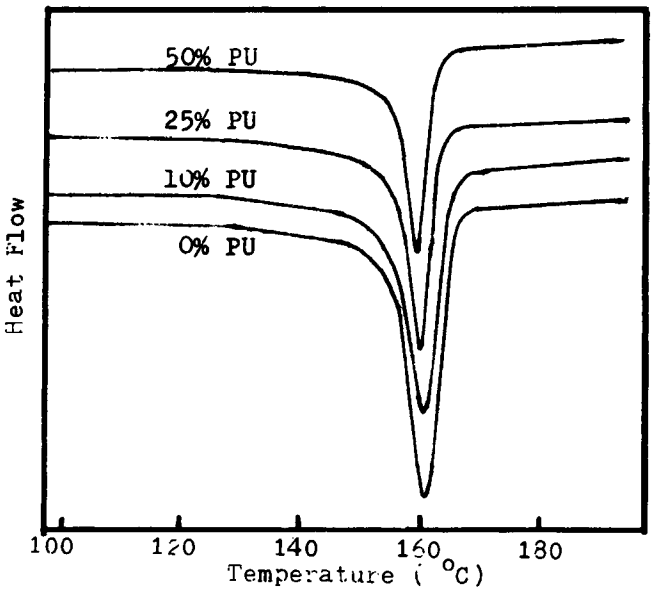

Fig. 7. Melting thermogram scan of polyblends of POM-I and PU, wt % of PU indicated on the curves.

and larger spherulitic structures. Thus, both Young's modulus and dielectric dissipation factor are a function of mobility. In Figure 6, within the range of small concentration of PU additives, $\tan\delta$ of the blend is in agreement with the additive valve, and then the $\tan\delta$ of the alloys rapidly increases with increasing concentration of PU.

Thermal Analysis

For the blends rich in POM, the melting peak temperature (T_m) and heat of fusion (H_f) obtained for three different compositions are shown in Figure 7 and Table I. It shows that the melting peak point of POM is not affected, and the heat of fusion of polyblend samples decreases with increasing the composition of PU. This is in good agreement with the density and crystallinity measurements.

TABLE I
Heat of Fusion (H_f), Degree of Crystallinity (X_c), Density, and Melting Temperature at Peak (T_m) for the Blend

Blend composition	H_f (J/g)	X_c (100%)	Density (g/cm^3)	T_m (°C)
0% PU	162.8	63.2	1.410	161.6
10% PU	143.1	55.4	1.384	161.5
25% PU	115.4	46.0	1.333	161.1
50% PU	86.6	30.8	1.248	160.5

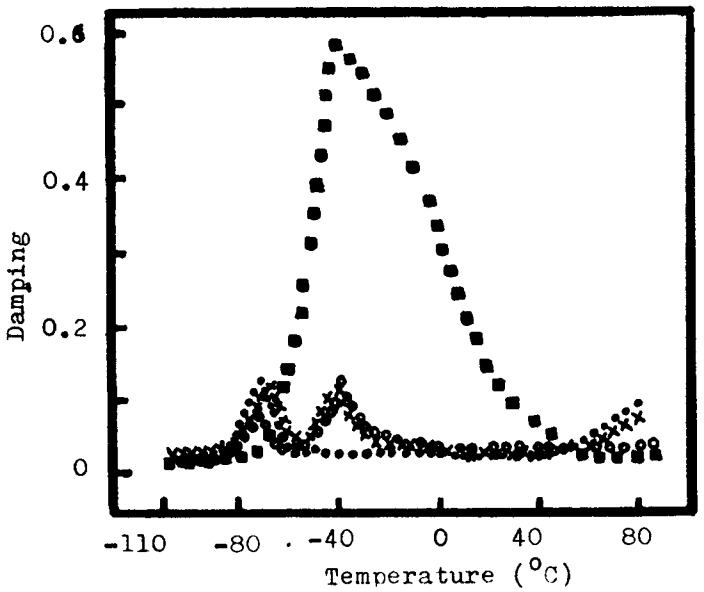

Fig. 8. Plots of damping vs. temperature: (●) POM; (×) POM/PU blend = 90/10 wt %; (○) POM/PU = 50/50 wt % (■) PU.

Dynamic Viscoelasticity

Figures 8–10 illustrate the dynamic mechanical properties curves of POM and PU as a function of temperature. From those figures, at the point where the modulus–temperature curves had an inflection point, the damping curves in Figure 8 went through a maximum. The loss modulus (E'') in Figure 10 is a term proportional to the energy dissipated as heat, which goes through a less

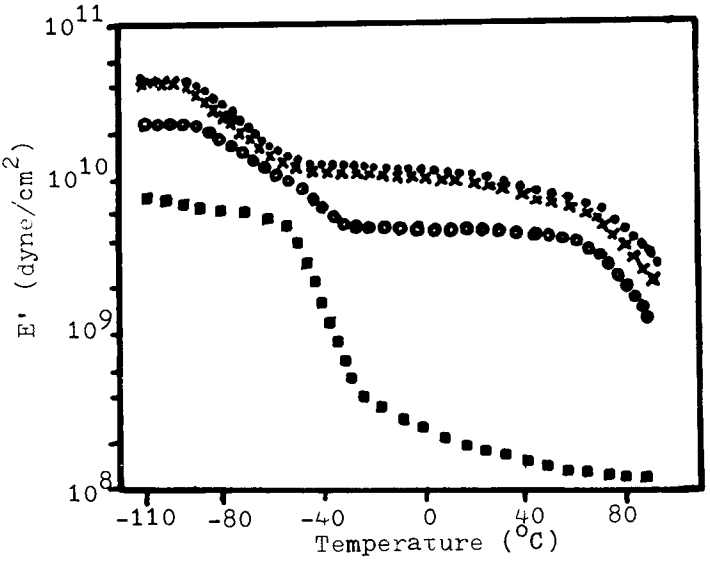

Fig. 9. Plots of storage modulus (E') vs. temperature: (●) POM; (×) POM/PU blend = 90/10 wt %; (○) POM/PU = 50/50 wt %; (■) PU.

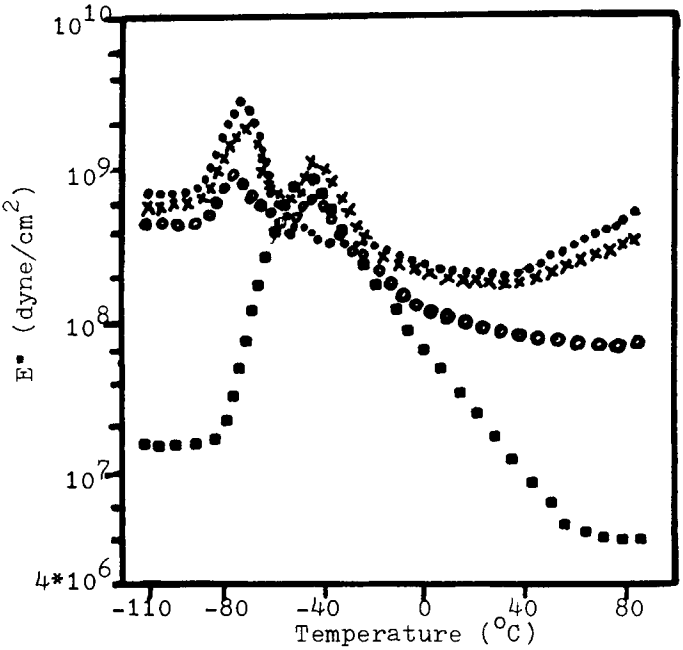

Fig. 10. Plots of loss modulus (E'') vs. temperature: (●) POM; (×) POM/PU blend = 90/10 wt %; (○) POM/PU blend = 50/50 wt %; (■) PU.

prominent peak than damping, and the maximum in the E'' curves occurred at a slightly lower temperature than the peak in the damping curves. The damping peak is associated with the partial loosening of the polymer structure so that small chain segments can move. In Figure 8 at a very low temperature (below -90°C for POM, -60°C for PU), the viscosity of both polymers is so high that the polymers are frozen and do not respond to force, and damping is very low. At a higher temperature (above -90°C for POM, -60°C for PU), the motion of both polymers increases. The glass transition temperature (T_g) of the POM and the PU are measured as T_g of POM = -73°C and T_g of PU = -47°C from Figure 10. The difference of glass transition temperature (ΔT_g) between the two polymers is 26°C.

In POM/PU blends rich in POM (90 wt %), the PU rubber particles disperse in the POM matrix, which shows that the T_g of POM is -71°C, and the T_g of PU is -48°C; so the difference of glass transition temperature (ΔT_g) for the blend is 24°C. Figure 11(B) indicates that the blend of POM/PU is not compatible. However, the T_g of POM is -75°C, and the T_g of PU is -47°C when the blend reaches 50 wt % PU. The difference of the glass transition temperature (ΔT_g) is -28°C in the blend, which indicates incompatibility between POM and PU (Fig. 10). The SEM in Figure 11(D-2) shows that the spherulite diameter of POM in the blend POM/PU (50/50 wt %) becomes smaller than the spherulite diameter of unblended POM in Figure 11(A-2). This lowers the T_g of POM below -75°C, because the amorphous region of POM in the blend slightly increases. Also, at higher PU concentration, the slope of the storage modulus curves (E'), as shown in Figure 9, decreases in the transition region.

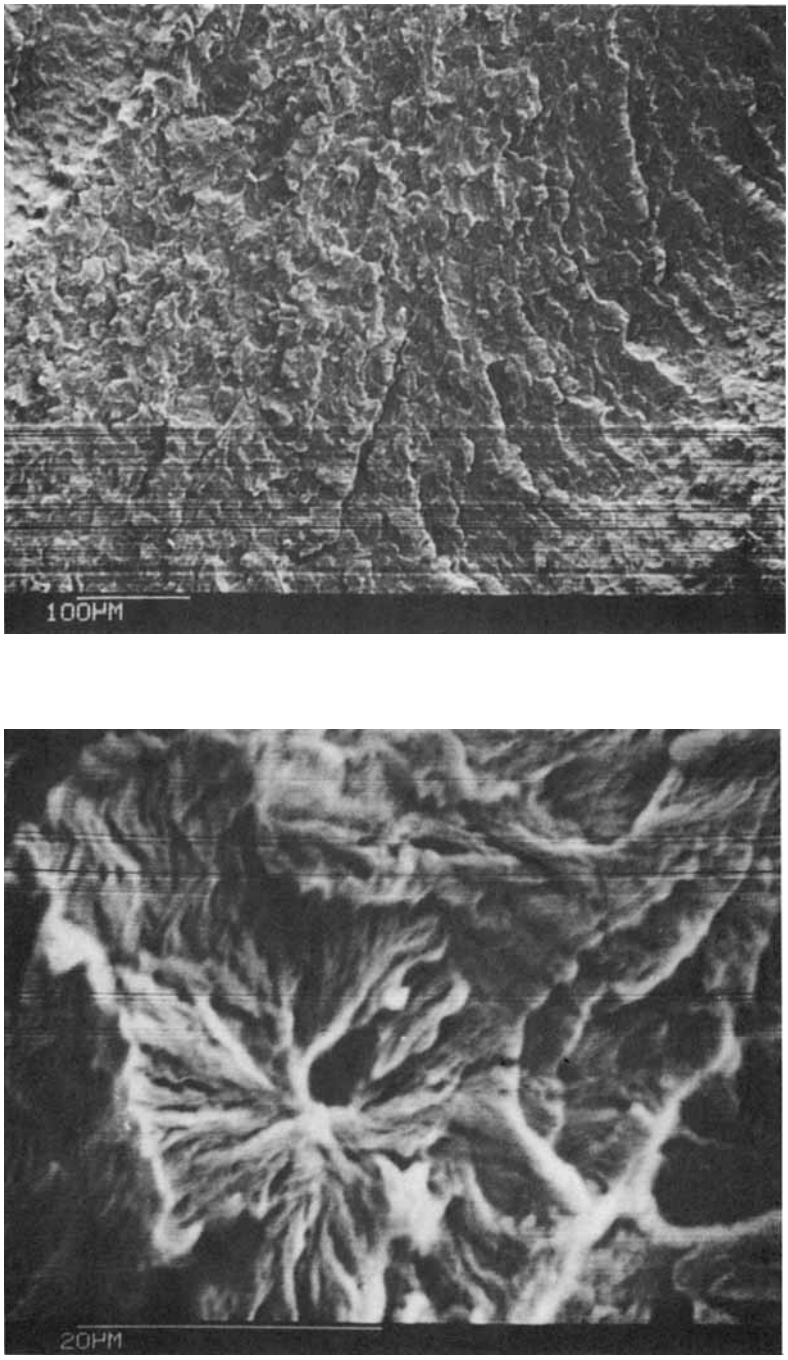

Fig. 11. SEM photomicrographs of POM/PU blends: (A-1, A-2) the unblended POM indicating the spherulite diameter about 20 μm; (B-1, B-2) POM/PU = 90/10 wt % blend; (C-1, C-2) POM/PU = 75/25 wt % blend; (D-1, D-2) POM/PU = 50/50 wt % blend showing the spherulite diameter of POM about 10 μm.

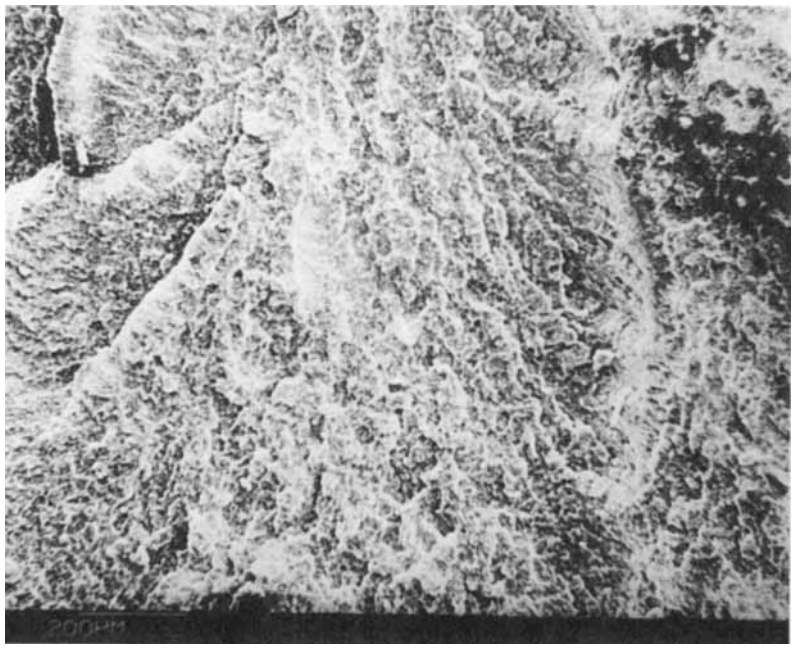

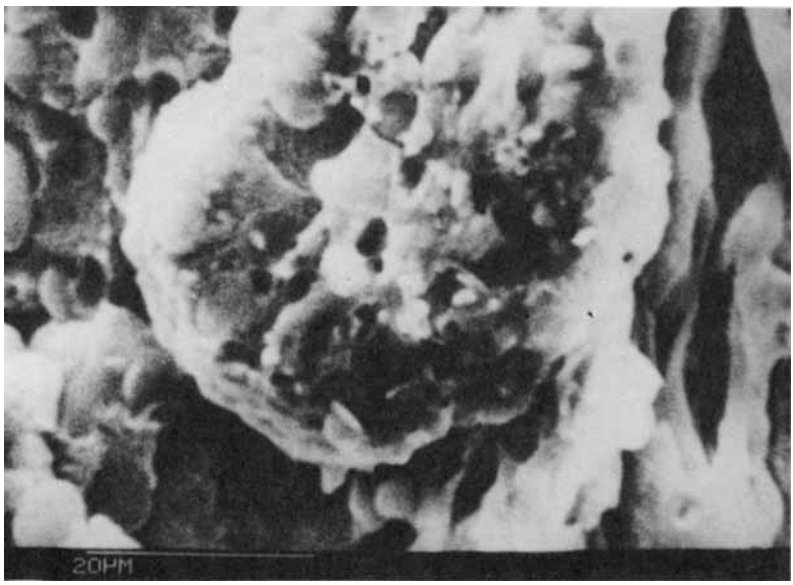

Fig. 11. (*Continued from the previous page.*)

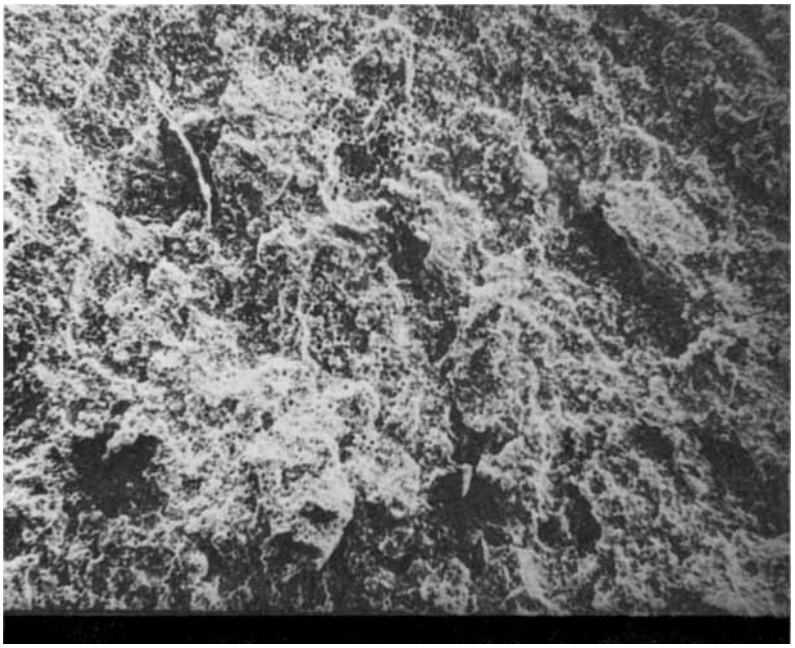

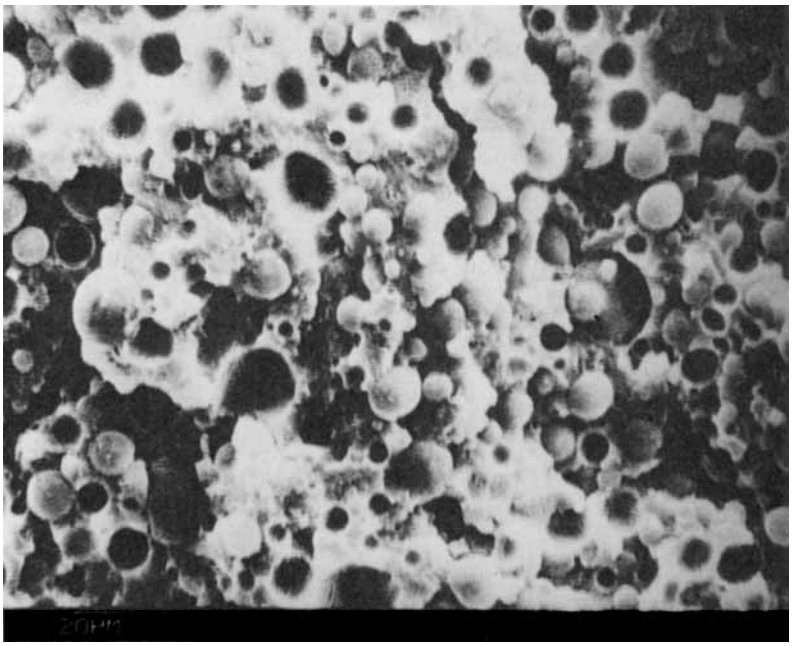

Fig. 11. (*Continued from the previous page.*)

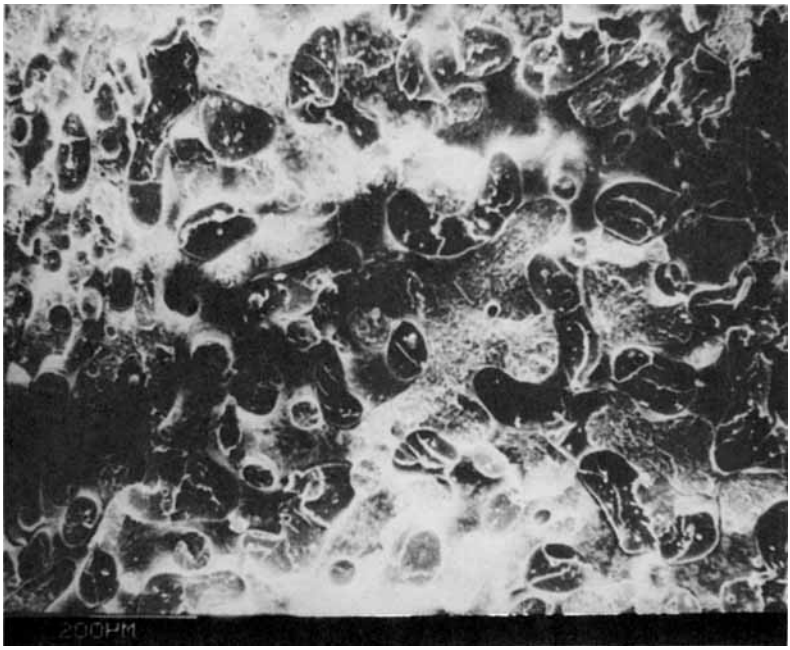

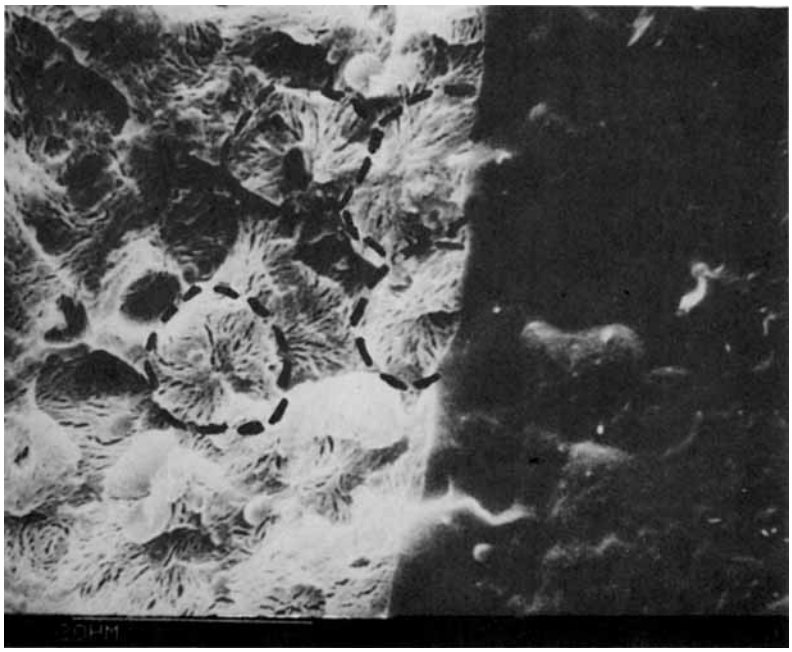

Fig. 11. (*Continued from the previous page.*)

Morphology

The morphology of cryofracture surfaces of the blends seem rather homogeneous, as observed by scanning electron microscopy (SEM). At the composition of 10 wt % PU [Fig. 11(B-1)], the spherical sizes of the dispersed PU in the POM matrix[22] are in the neighborhood of 1–3 μm in diameter, and the spherulites of POM become less perfect with coarse fine structure as shown in Figure 11(B-2) in comparison with that of unblended POM in Figure 11(A-2). At a composition of 25 wt % PU, the alloy exhibits larger spherical domains of PU from 5 to 10 μm with poor adhesion to the POM matrix, as shown in Figure 11(C). The ultimate tensile strength at a composition of 10 wt % PU is lower than that of unblended POM, whereas the elongation at break and impact strength increase remarkably. The morphology of the PU phase affects the impact strength because PU acts as an energy absorber and improves the impact strength of the blend. The PU particles are spherical in shape with spherical inclusions of the POM matrix. This is probably due to a decrease in free energy at larger domain sizes, since larger domains produce a lower surface area per unit volume. A minimum exists, therefore, in the free energy at a certain domain size which depends on the particular morphology. Spherical particles of dispersed PU have the lowest energy at the highest composition.[23] The observation of POM/PU blends containing lower than 50 wt % PU is also in agreement with the morphology of the blends.[2,10,13,14]

At a concentration of 50 wt % PU, however, the dispersed PU particles tend to agglomerate and to form elongated rather than spherical particles as shown in Figure 11(D-1). From the morphology study, the boundaries between POM phase and PU phase become clear; moreover, the discrete phase of POM in the blend denoted by light regions indicates that the effect of the PU phase results in an enhanced nucleation rate[6] and a decrease in the average size of spherulites of POM. Therefore, the average spherulite diameter of POM in the blend about 10 μm [Fig. 11(D-2)] is smaller than those of the unblended POM [Fig. 11(A-2)], which is about 20 μm.

Reduction in spherulite size was observed by Lovinger and Williams[14] for high density polyethylene (HDPE) and polypropylene (PP) blends on microtomed sections of the bulk sample. In the case of PP and polybutene-1 (PB) blend, Siegmann[10] also made the same observation, where the thin film crystallized blends gave a mixture of small crystalline aggregates similar in appearance to those observed for isotactic polystyrene (iPS)/atactic polystyrene (aPS) and isotactic polypropylene (iPP)/atactic polypropylene (aPP) blends.[23] However, no spherulitic morphology has been reported for SEM or optical photomicrographs of PE/PB,[2] PP/PB,[10] poly(ethylene terephthalate) (PET)/poly(butylene terephthalate) (PBT),[24] iPS/APS, and iPP/aPP[23] blends with two crystallizable components containing 50 wt % in the blend each.

CONCLUSION

In general, from bulk samples of POM/PU blends rich in POM, the properties of the blends are evidence of various degrees of mutual influence of the two components. The important factor deciding whether properties are enhanced through blending is the miscibility and interaction between the two

components. This consideration determines the resultant structure of the blend and hence controls their properties. Melt blending of POM/PU gave a blend consisting of spherulites of POM. Mechanical properties show that impact strength of POM/PU blends increased with decreasing spherical size of the dispersed PU. This is not a compatible situation but only controlled dispersion so that morphology dictates crack propagation.

From WAXD studies, the diffraction line measured at half POM maximum intensity was not affected by blend composition, suggesting that there is no change in the crystal lamellar thickness[19] of POM. Furthermore, in the POM/PU (50/50 wt %) blends, we observed a small spherulitic morphology of polymer (POM) which could not be observed from microscopy made on crystallized thin film.[2,3,10,14,24,25] Finally, it has been recognized that the properties of blends strongly depend on the morphology, that is, on miscibility, size and form of dispersed phase, character, and size of the interphase domain.

The authors wish to express their appreciation to Dr. T. S. Lin, the President of the Tatung Institute of Technology, for his encouragement and support.

References

1. Wen-Yen Chiang and Dao-Shinn Hwung, *Polym. Eng. Sci.*, **27**, 632 (1987).
2. K. Kishore and R. Vasanthakumari, *Polymer*, **27**, 337 (1986).
3. J. W. Teh, *J. Appl. Polym. Sci.*, **28**, 605 (1983).
4. A. Siegmann, *J. Appl. Polym. Sci.*, **27**, 1053 (1982).
5. R. Fayt, R. Jerome, and Ph. Tessie, *J. Polym. Sci., Polym. Phys. Ed.*, **20**, 2209 (1982).
6. E. Martucelli, C. Silvestre, and G. Abate, *Polymer*, **23**, 229 (1982).
7. A. K. Gupta, V. B. Gupta, R. H. Petters, W. G. Harland, and J. P. Berri, *J. Appl. Polym. Sci.*, **27**, 4669 (1982).
8. R. Fayt, R. Jerome, and P. Teyssie, *J. Polym. Sci., Polym. Phys. Ed.*, **19**, 1269 (1981).
9. F. L. Slagowski, E. P. Chang, and J. Tkacik, *J. Polym. Eng. Sci.*, **21**, 513 (1981).
10. A. Siegmann, *J. Appl. Polym. Sci.*, **24**, 2333 (1979).
11. B. Schnerier, *J. Appl. Polym. Sci.*, **18**, 1999 (1974).
12. A. Foglia, *J. Appl. Polym. Symp.*, **11**, 1 (1969).
13. S. Bywater, *Polym. Eng. Sci.*, **24**, 104 (1984).
14. A. J. Lovinger and M. L. Williams, *J. Appl. Polym. Sci.*, **25**, 1703 (1980).
15. Y. Lipatov, *Pure Appl. Chem.*, **43**, 273 (1975).
16. M. Baer, *J. Appl. Polym. Sci.*, **16**, 1109, 1125 (1972).
17. B. W. Bender, *J. Appl. Polym. Sci.*, **9**, 2887 (1965).
18. G. Cigna, *J. Appl. Polym. Sci.*, **14**, 1781 (1970).
19. E. R. Wagner and L. M. Robeson, *Rubber Chem. Technol.*, **43**, 1129 (1980).
20. H. D. Keith and F. J. Padden, *J. Appl. Phys.*, **35**, 1270 (1975).
21. C. J. Ong and F. P. Price, *J. Polym. Sci. Symp.* **63**, 45 (1978).
22. F. Kloos and E. Wolter, *Kunststoffe*, **75**, 735 (1985).
23. H. D. Keith and F. J. Padden, *J. Appl. Phys.*, **35**, 1270 (1964).
24. R. S. Stein, F. B. Khambatta, F. P. Warner, T. Russell, A. Escala, and E. Balizer, *J. Polym. Sci. Polym. Symp.*, **63**, 313 (1978).

Received July 23, 1987
Accepted December 28, 1987